International Journal of Computer Assisted Radiology and Surgery (2020) 15:1279–1290
https://doi.org/10.1007/s11548-020-02154-7

ORIGINAL ARTICLE

A statistical weighted sparse-based local lung motion modelling approach for model-driven lung biopsy

Dong Chen[1,2,3] · **Hongzhi Xie**[4] · **Lixu Gu**[5] · **Wei Guo**[1,2,3] · **Liang Tian**[1,2,3] · **Jing Liu**[1,2,3]

Received: 20 October 2019 / Accepted: 3 April 2020 / Published online: 28 April 2020
© CARS 2020

Abstract

Purpose Lung biopsy is currently the most effective procedure for cancer diagnosis. However, respiration-induced location uncertainty presents a challenge in precise lung biopsy. To reduce the medical image requirements for motion modelling, in this study, local lung motion information in the region of interest (ROI) is extracted from whole chest computed tomography (CT) and CT-fluoroscopy scans to predict the motion of potentially cancerous tissue and important vessels during the model-driven lung biopsy process.

Methods The motion prior of the ROI was generated via a sparse linear combination of a subset of motion information from a respiratory motion repository, and a weighted sparse-based statistical model was used to preserve the local respiratory motion details. We also employed a motion prior-based registration method to improve the motion estimation accuracy in the ROI and designed adaptive variable coefficients to interactively weigh the relative influence of the prior knowledge and image intensity information during the registration process.

Results The proposed method was applied to ten test subjects for the estimation of the respiratory motion field. The quantitative analysis resulted in a mean target registration error of 1.5 (0.8) mm and an average symmetric surface distance of 1.4 (0.6) mm.

Conclusions The proposed method shows remarkable advantages over traditional methods in preserving local motion details and reducing the estimation error in the ROI. These results also provide a benchmark for lung respiratory motion modelling in the literature.

Keywords Statistical respiratory motion model · Weighted sparse algorithm · Motion prior-based registration · Computed tomography

Introduction

Lung biopsy is typically required for a definitive diagnosis of potential cancer; however, the problem of organ motion caused by respiration leads to position uncertainty in the lung, thus greatly degrading the success rate of lung biopsy [1]. Moreover, it has recently been shown that the geometry of significant blood vessels in the lung will result in clinically significant internal bleeding if such vessels are punctured [2]. It is therefore crucial to be able to accurately predict the respiratory motion of the region of interest (ROI), such as the tumour and nearby vessel structures.

Many tracking strategies, including both image- and model-driven approaches, are currently used in clinical biopsy practice. Image-driven approaches rely on a variety of intra-interventional imaging techniques, such as X-ray fluoroscopy, magnetic resonance imaging (MRI), computed

---

✉ Liang Tian
tianliang@chmiot.net

✉ Jing Liu
liujing001@ict.ac.cn

[1] College of Computer and Cyber Security, Hebei Normal University, Shijiazhuang, China

[2] Key Laboratory of Network and Information Security, Hebei Normal University, Shijiazhuang, China

[3] Key Laboratory of Augmented Reality, School of Mathematical Sciences, Hebei Normal University, Shijiazhuang, China

[4] Department of Cardiothoracic Surgery, Peking Union Medical College Hospital, Beijing, China

[5] Laboratory of Image Guided Surgery and Therapy (IGST), Shanghai Jiao Tong University, Shanghai, China

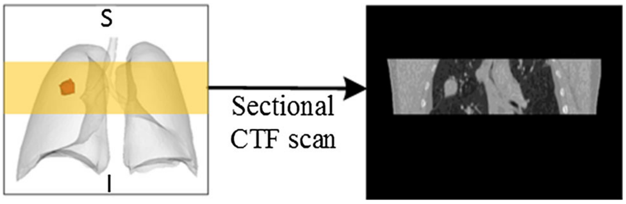

Fig. 1 Example of a sectional CTF scan of a tumour region

tomography (CT) and CT-fluoroscopy (CTF), for tumour and ROI tracking [3]. However, real-time X-ray fluoroscopy provides only a 2D projective image and has low image contrast in lung tissue. MRI scans are not always feasible in clinical practice due to their high cost and complex procedure. By contrast, volumetric CT scans can produce high-quality 3D images and are widely applied in clinical settings. CTF scans, which can generate a limited number of 2D axial images in the superior–inferior (SI) direction, are often employed to guide percutaneous lung interventions (see Fig. 1). However, in traditional CT- and CTF-guided lung biopsy, physicians must frequently capture medical images to modify the positioning of the biopsy needle, which may result in unnecessary radiation exposure for both patients and physicians. Compared to the image-guided strategy, model-driven biopsy approaches can effectively avoid this additional scan dose during lung intervention because only surrogate signals need to be acquired to drive the model for motion predication during clinical lung intervention. One of the possible workflows for applying this approach to the clinical lung biopsy is proposed in our previous work [4]: a reference needle is first positioned in the region near the ROI by a thoracic surgeon before the operation. The location of the reference needle, which is used as the surrogate signal to drive the motion model to predict the tumour position, can be determined in medical images. Then, CT image pairs are acquired at different breathing phases to extract the deformation vector fields (DVFs) for motion modelling, and the coordinate system of the motion model is aligned to the real operation space based on skin markers. During the biopsy process, the real location of the reference needle can be tracked by an electromagnetic navigator. The aligned motion model is used to determine the current breathing phase by simulating a similar location of the reference needle with its real location, and predict the motion information associated with the tumour and ROI.

Image registration-based methods and statistical methods are promising techniques for handling the motion prediction task. Traditionally, image registration-based methods are performed by minimizing the intensity information between image pairs consisting of fixed and floating medical images to extract DVFs that describe the temporal change in the position of interest. Although many machine learning-based methods for 2D–2D, 2D–3D and 3D–3D image registration have been proposed in recent years [5, 6], it is a challenging task to register CTF images with CT images to directly extract motion information. To overcome the problem of regular registration, Su et al. [3] proposed a fast CT–CTF registration algorithm with respiratory motion compensation. However, the proposed registration framework limited the displacement of the control point in the SI direction, which introduced unnecessary estimation error. In addition, the need for two preprocedural CT scans resulted in additional radiation exposure and costs.

However, the registration of different-size image pairs with large deformations remains a challenging task. In contrast, a statistical motion model is formed on the basis of motion data acquired from training images that can be adapted for the prediction of patient-specific motion with a reduced need for additional imaging data. Such a model can also serve as a motion prior during the traditional registration process to reduce deformation between intermediate CT and CTF images to improve the accuracy of registration [3]. For the construction of such a model, the DVFs of several 4D image datasets are extracted using nonlinear intensity-based registration methods. In most studies, these models are based on a principal component analysis (PCA). An exception is the work conducted by Ehrhardt et al. [7], who used a statistical 4D mean motion model (MMM) to estimate lung respiratory motion based on the assumption that breathing dynamics are similar for different patients. However, this assumption is unrealistic because the motion patterns of different subjects typically differ [8, 9]. In the PCA-based modelling approach, a set of volumetric images captured in different breathing phases is used to extract DVFs, and new volumetric images are reconstructed based on the reference images by varying a few eigenvectors and coefficients. Ha et al. [10] introduced a dense patient-specific motion model by performing a PCA of the estimated displacement fields with a unified discrete optimization framework. Similarly, Samei et al. [11] proposed the use of exemplar population models to generate an adaptable population model for the prediction of liver motion based on a PCA and 4D motion fields obtained from several 4D MRI datasets. Instead of predicting respiratory motion based on either a PCA subject-specific model or a PCA population model, this method considered the dissimilarity among three manually determined points and the corresponding components of each PCA subject-specific model to formulate weight coefficients. Finally, the motion vectors of the manually determined points were approximately represented by a linear combination of the exemplar models. However, the discarded eigenvectors in a PCA model are statistically nonsignificant and often contain important local motion details [12]. The sparse representation method proposes a potential approach to lung segmentation [13] and motion analyses [14–16]. In our previous work, we proposed a lung motion prediction framework based on a sparse representation method using two orthogonal X-ray images and a pre-operative CT [15, 16]. The DVFs of several image datasets are first extracted to construct a respiratory motion repository (see "Data preparation" section for more details). The respiratory motion of a new input patient can be represented as a linear combination of DVFs in this motion respiratory with a set of sparse coefficients based on the sparse representation method, and the sparse coefficients will be optimized by maximizing the image similarity between the X-ray images and the projection image of the deformed CT, which were generated based on the pre-operative CT with the motion information. However, the X-ray image provides only a 2D projective image and has low image contrast in lung tissue, thus may fail to clearly visualize the internal lung structure and lead to the modelling method achieved an unstable motion prediction performance of the entire lung, especially for the vessel structures. In addition, since the motion patterns of different types of respiration typically differ, the motion information of training DVFs has a wide range of variation. A potential problem associated with the traditional sparse algorithm-based method [13–16] is that the respiratory motion information for the new input patient is probably formulated with a training DVF that represents a different motion pattern from the new input one, and thus may also influence the motion prediction accuracy.

To overcome this issue, we introduce a motion prediction framework for model-driven lung biopsies in which preprocedural whole chest CT and intraprocedural CTF images acquired at different time points are used to extract motion information in the ROI rather than the X-ray images. The major contributions include the following. (1) A weighted sparse algorithm-based statistical motion modelling method is proposed. This method can automatically generate more discriminative sparse weights and composite several training DVFs that have similar motion information with new input specific to the patient to provide a more robust and accurate motion predication than the traditional sparse algorithm-based method [13–16]. (2) Combined with the prior information, a motion prior-based registration method is designed to improve the prediction accuracy in the ROI. In addition, an adaptive variable coefficient approach is designed to balance the influence of the prior knowledge with that of the image intensity information during the registration process.

Materials and methods

A flow diagram of the proposed motion modelling framework is shown in Fig. 2. The patient-specific DVFs used for the training datasets, which are extracted using a nonlinear registration method, are employed to construct the respiratory motion repository (DVFs) for the proposed motion modelling method. The mapping matrix $\varphi_{1\rightarrow p}$ from the CT images $I_{\mathrm{CT},1}$ of $Subject\ 1$ to the images $I_{\mathrm{CT},p}$ of $Subject\ p$ ($p = 2, 3, \ldots, n$) is generated based on a registration method (see "Data preparation" section for more details). In "Weighted sparse algorithm-based statistical motion model" section, given the EI CT ($I_{\mathrm{CT},j}$) and EE CTF images from a new input $Patient\ j$, the mapping matrix $\varphi_{j\rightarrow 1}$ is generated using a registration method for warping the images $I_{\mathrm{CT,j}}$ onto the EI CT reference images $I_{\mathrm{CT,1}}$ in the training datasets. Subsequently, an automatic segmentation method is employed to generate the lung vessel surface $S_{\mathrm{CT},j}$ and $S_{\mathrm{CTF},j}$ of $Patient\ j$. Combined with the mapping matrix $\varphi_{j\rightarrow 1}$ and $\varphi_{1\rightarrow p}$, the corresponding position of $S_{\mathrm{CT},j}$ can be determined in the pth training image region and is denoted as $S'_{\mathrm{CT},p}$. Thus, the corresponding respiratory motion M will be generated with the resulting DVFs. The weighted sparse algorithm-based statistical motion modelling method is then applied to obtain a unique set of sparse weight coefficients, thus generating a patient-specific DVF for the current patient to describe the motion of the tissue in the lung. Finally, an accurate local motion model of the ROI is generated using the prior motion information via the motion prior-based registration method ("Motion prior-based registration with adaptive variable coefficients" section).

Data preparation

In this study, a motion repository was constructed from CT training datasets acquired from 26 training subjects during the EE and EI phases. Nine subjects exhibited diaphragmatic respiration, and the remaining subjects exhibited some thoracic-related respiration behaviour. The spatial resolution of each volumetric image was $0.912 \times 0.912 \times 1.25$ mm with a spatial resolution of $512 \times 512 \times 256$ voxels. All datasets were acquired at Peking Union Medical College Hospital. The CT image coordinate system of different subjects was transformed into a common coordinate system by alignment of the vertebral bodies. Given a set of aligned training CT image pairs, a nonparametric discrete registration method [17] was employed to extract the DVF information from the aligned EI to EE CT images. Thus, the construction of the motion repository can be presented as follows: $\mathrm{DVF}_s = [\mathrm{DVF}_1, \mathrm{DVF}_2, \ldots, \mathrm{DVF}_n]$, where the DVF of $Subject\ p$ is denoted as DVF_p ($p = 1, 2, \ldots, n$), and $n = 26$ is the number of training subjects in the lung motion repository.

Weighted sparse algorithm-based statistical motion model

For the construction of a respiratory motion model, an automatic segmentation method [18] is first employed to segment the lung vessel from the new input EI CT image $I_{\mathrm{CT},j}$ and EE CTF image $I_{\mathrm{CTF},j}$ of $Patient\ j$. Let $S_{\mathrm{CT},j}$ and $S_{\mathrm{CTF},j}$

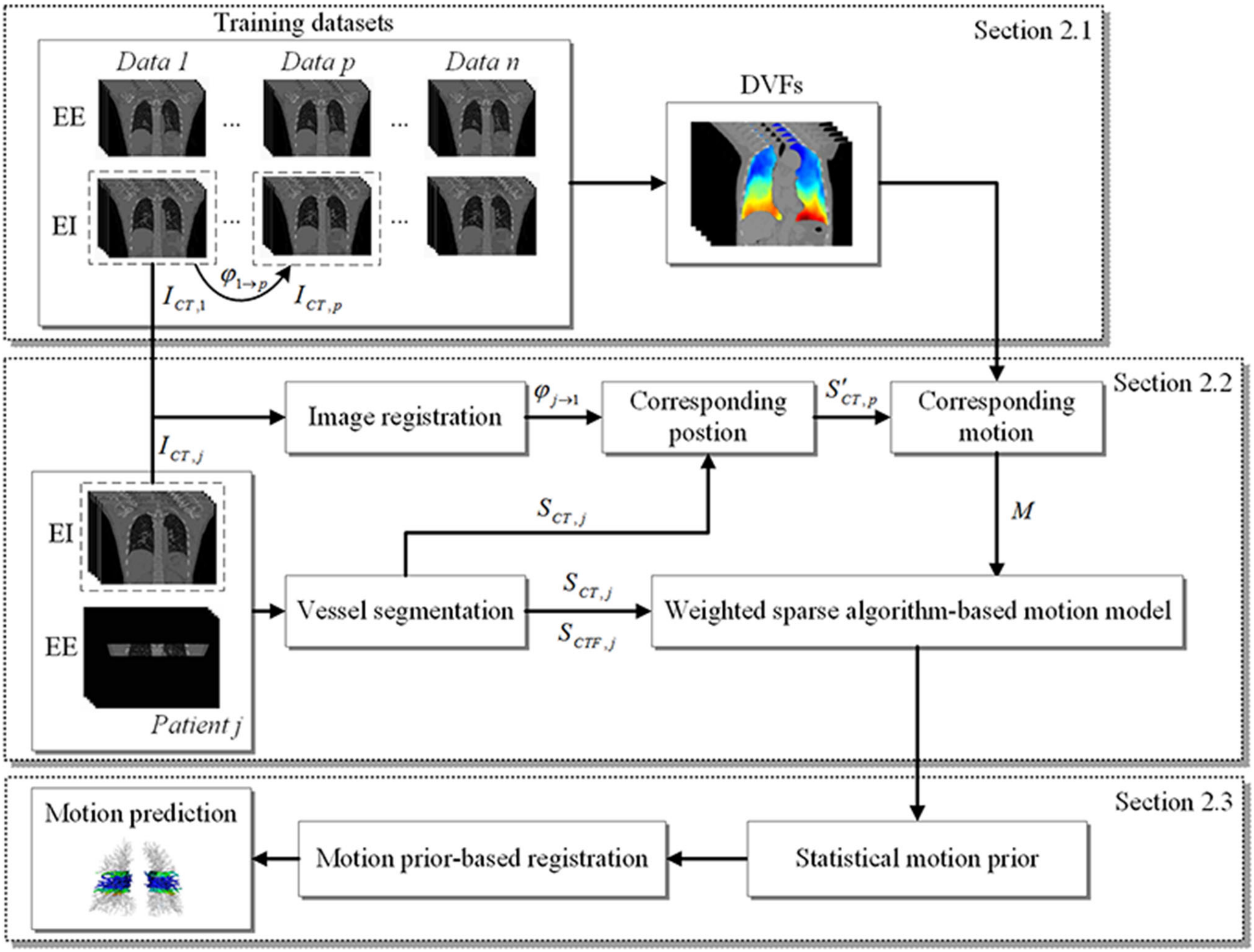

Fig. 2 Framework of lung respiratory motion estimation based on EI CT images and EE CT images

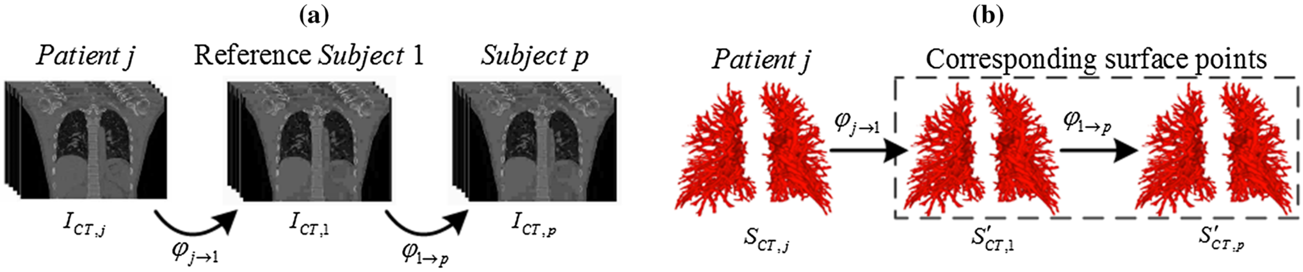

Fig. 3 Overview of the generation of corresponding surface points for the new input of *Patient j*. **a** First, a registration method is employed to compute the transformations $\varphi_{j\to 1}$ and $\varphi_{1\to p}$ for warping the image $I_{\mathrm{CT},j}$ to reference image $I_{\mathrm{CT},1}$ and image $I_{\mathrm{CT},p}$ of *Subject p*. **b** The corresponding surface points of the lung surface of *Patient j* are determined based on these resulting transformations and $S_{\mathrm{CT},j}$

denote the vessel surface in the EI CT and EE CTF images, respectively. We then randomly select a reference image from among the training datasets. For instance, suppose that the CT image $I_{\mathrm{CT},1}$ of *Subject 1* is chosen as the reference image. The transformation $\varphi_{j\to 1}$ between the image $I_{\mathrm{CT},j}$ of *Patient j* and the reference image $I_{\mathrm{CT},1}$ can be generated using the registration method [17], as shown in Fig. 3a. In Fig. 3b, the transformation $\varphi_{j\to 1}$ was used to transform the surface points on $S_{\mathrm{CT},j}$ to their corresponding points $S'_{\mathrm{CT},1}$ in $I_{\mathrm{CT},1}$: $S'_{\mathrm{CT},1} = \varphi_{j\to 1}(S_{\mathrm{CT},j})$. Similarly, the corresponding points $S'_{\mathrm{CT},p}$ of the surface points $S'_{\mathrm{CT},1}$ can be determined in the image region of *Subject p* by using the transformation $\varphi_{1\to p}$ between the reference image $I_{\mathrm{CT},1}$ and the image $I_{\mathrm{CT},p}$ of *Subject p* as $S'_{\mathrm{CT},p} = \varphi_{1\to p}(S'_{\mathrm{CT},1})$.

The motion information $M = [m_1, m_2, \ldots, m_n] \in \Re^{k\times n}$ is then generated from the $S'_{\mathrm{CT},p}$ using the corresponding DVFs ("Data preparation" section). Each column of M is a vector representing the motion of k points of surface $S'_{\mathrm{CT},p}$. The modelling method aims to find a deformed vessel tree surface $S_{\mathrm{CT},j} + M\mu$ that is close to the target surface $S_{\mathrm{CTF},j}$ by seeking the appropriate sparse weights $\mu = \left[\mu_1, \mu_2, \ldots, \mu_n\right]^{\mathrm{T}} \in \Re^{n\times 1}$. The deformation of all surface points on the $S_{\mathrm{CT},j}$ can be represented as $M\mu$, which indicates a linear combination of the motion of surface points in M. However, the resulting transformations $\varphi_{j\to 1}$ and $\varphi_{1\to p}$ will inevitably introduce errors that will influence the locations of the corresponding surface points $S'_{\mathrm{CT},1}$ and $S'_{\mathrm{CT},p}$. To alleviate this problem, we explicitly model this error of k surface points as a sparse vector $e \in \Re^{k\times 1}$. The optimization function of the modelling method is formulated as follows:

$$\arg\min_{\mu,e} f_e\left(S_{\mathrm{CTF},j}, S_{\mathrm{CT},j} + M\mu - e\right) + \lambda_1 \|\mu\|_1 + \lambda_2 \|e\|_1, \tag{1}$$

$$f_e\left(S_{\mathrm{CTF},j}, S_{\mathrm{CT},j} + M\mu - e\right) = \frac{1}{t}\sum_{z=1}^{t} \min_{s^z_{\mathrm{CTF},j}\in S_{\mathrm{CTF},j}} \left\| s^z_{\mathrm{CTF},j} - \left(S_{\mathrm{CT},j} + M\mu - e\right)\right\|, \tag{2}$$

where the symbols λ_1 and λ_2 are predefined sparsity numbers that control the sparseness of μ and e. f_e is the similarity energy used to measure the shortest Euclidean distance from the zth surface point ($s^z_{\mathrm{CTF},j}$) on the target surface $S_{\mathrm{CTF},j}$ to the closest point on the deformed surface $S_{\mathrm{CT},j} + M\mu - e$, and the symbol t indicates the number of surface points on $S_{\mathrm{CTF},j}$. Furthermore, we employ a normalized diagonal matrix, $W = \mathrm{diag}[w_1, \ldots, w_n] \in \Re^{n\times n}$, to characterize the similarity of internal motion between the new input patient and each training subject.

$$\arg\min_{\mu,e} f_e\left(S_{\mathrm{CTF},j}, S_{\mathrm{CT},j} + M\mu - e\right) + \lambda_1 \|W\mu\|_1 + \lambda_2 \|e\|_1, \tag{3}$$

$$W = \frac{\mathrm{diag}\left(\left[f_e(S_{\mathrm{CTF},j}, S_{\mathrm{CT},j} + \alpha_1 m_1), \ldots, f_e(S_{\mathrm{CTF},j}, S_{\mathrm{CT},j} + \alpha_p m_p), \ldots, f_e(S_{\mathrm{CTF},j}, S_{\mathrm{CT},j} + \alpha_n m_n)\right]\right)}{\max\left(f_e(S_{\mathrm{CTF},j}, S_{\mathrm{CT},j} + \alpha_1 m_1), \ldots, f_e(S_{\mathrm{CTF},j}, S_{\mathrm{CT},j} + \alpha_p m_p), \ldots, f_e(S_{\mathrm{CTF},j}, S_{\mathrm{CT},j} + \alpha_n m_n)\right)}. \tag{4}$$

The vessel surface motion amplitude of each training subject $Subject\ p$ is controlled by the parameter α_p to eliminate the influence of the individual depth of respiration. The value of α_p can be computed before solving the objective function. If the resulting value of w_p is small, the DVF of $Subject\ p$ will be considered to have a similar breath pattern and will be chosen preferentially to present the DVF of the new input patient $Patient\ j$. The solution for μ in Eq. 3 is equivalent to $W^{-1}\hat{\mu}$, where $\hat{\mu}$ is calculated using the following optimization function:

$$\arg\min_{\hat{\mu},e} f_e\left(S_{\mathrm{CTF},j}, S_{\mathrm{CT},j} + MW^{-1}\hat{\mu} - e\right) + \lambda_1 \left\|\hat{\mu}\right\|_1 + \lambda_2 \|e\|_1 . \tag{5}$$

This optimization problem can be solved using the fast iterative shrinkage-thresholding algorithm (FISTA) [19]. The basic statistical respiratory motion model formulation can be used to approximately represent the respiratory motion field $\mathrm{DVF}_j(x_i)$ of any new input patient as a weighted linear combination of the fields in the motion repository, $\mathrm{DVF}_p(x_i)$, as follows: $\mathrm{DVF}_j(x) = \sum_{p=1}^{n} \mathrm{DVF}_p(x)\cdot\hat{\mu}_p$, where x denotes a voxel in the image space. We further optimize the weight coefficients $\hat{\mu}$ based on the image similarity energy, which measures the region of overlap between the new inputs $I_{\mathrm{CT},j}$ and $I_{\mathrm{CTF},j}$. Therefore, the influence of the inter-registration error will be further eliminated.

$$\arg\max_{\hat{\mu}} \mathrm{Sim}\left[I_{\mathrm{CTF},j}, I_{\mathrm{CT},j}\left(x + \sum_{p=1}^{n}\mathrm{DVF}_p(x)\cdot\hat{\mu}_p\right)\right], \tag{6}$$

where Sim represents the normalized mutual information similarity between the target CTF image $I_{\mathrm{CTF},j}$ and the deformed CT image $I_{\mathrm{CT},j}\left(x + \sum_{p=1}^{n}\mathrm{DVF}_p(x)\cdot\hat{\mu}_p\right)$ under the current deformation $\sum_{p=1}^{n}\mathrm{DVF}_p(x)\cdot\hat{\mu}_p$. The optimal sparse weight coefficients $\hat{\mu} = \left[\hat{\mu}_1, \hat{\mu}_2, \ldots, \hat{\mu}_n\right]^{\mathrm{T}} \in \Re^{n\times 1}$ can be obtained via the gradient descent method with one of the nonzero weight coefficients as variable and the others as fixed. Thus, the deformation field $\mathrm{DVF}_j(x)$ of the new input data can be approximately reconstructed used as the motion prior $g_{\mathrm{prior}}(x)$ in the motion prior-based registration process.

$$g_{\mathrm{prior}}(x) = \mathrm{DVF}_j(x) = \sum_{p=1}^{n}\mathrm{DVF}_p(x)\cdot\hat{\mu}_p. \tag{7}$$

Motion prior-based registration with adaptive variable coefficients

The motion prior $g_{\text{prior}}(x)$ is employed to generate a deformed CT image $I_{\text{CT},j}\left(x + g_{\text{prior}}(x)\right)$ to reduce the deformation between the source CT image $I_{\text{CT},j}$ and the CTF image $I_{\text{CTF},j}$ of a new patient j. An iterative refinement process is implemented to improve the prediction accuracy in the ROI by minimizing the following objective function:

$$\arg \min_{\mu_p^*, g(x)} \sum_{x \in \Omega} \left[I_{\text{CTF},j} - I_{\text{CT},j} \left(x + \sum_{p=1}^{n} \text{DVF}_p(x) \cdot \mu_p^* + g(x) \right) \right]^2 + \sum_{x \in \Omega} g\left(x^{\text{SI}}\right)^2, \tag{8}$$

where x denotes a voxel in the image space Ω, $g(x)$ is the displacement of the deformation field obtained through B-spline registration and $g(x^{\text{SI}})$ represents the displacement $g(x)$ in the superior–inferior (SI) direction. The initial sparse weights $\hat{\mu}$ of the motion prior $g_{\text{prior}}(x)$ are first further fine tuned to seek the optimal weights μ^* by best matching the deformed CT image $I_{\text{CT},j}\left(x + \sum_{p=1}^{n} \text{DVF}_p(x) \cdot \mu_p^* + g(x)\right)$ with the reference image $I_{\text{CTF},j}$, where $g(x) = 0$ in the first iterative process. Subsequently, the displacement $g(x)$ of the deformation field between the reference images $I_{\text{CTF},j}$ and deformed CT image $I_{\text{CT},j}\left(x + \sum_{p=1}^{n} \text{DVF}_p(x) \cdot \mu_p^* + g(x)\right)$ with the resulting value μ^* is computed via image registration. Since CTF scans can be regarded as a limited number of 2D axial images in the SI direction and provide full coverage of the image region in the other two directions, the displacement $g(x)$ near the boundary of CTF images along the SI direction should be regularized by using $\sum_{x \in \Omega} g(x^{\text{SI}})^2$.

During the above iterative process, the weights μ^* are employed to obtain more suitable motion prior information to improve the accuracy of the motion prediction near the boundary of the CTF images. Then, an appropriate value $g(x)$ can provide motion information that is lost in the weight sparse model. The final motion information of $Patient\ j$ can be presented as follows: $\sum_{p=1}^{n} \text{DVF}_p(x) \cdot \mu_p^* + g(x)$. Notably, both $\sum_{p=1}^{n} \text{DVF}_p(x) \cdot \mu_p^*$ and $g(x)$ represent the deformation field in the 3D CT image space and can be directly added. In the B-spline registration method, each control node influences only a subregion of the image. We can design a set of adaptive variable coefficients to provide a suitable penalty in the following function:

$$\arg \min_{\mu_p^*, g(x)} \sum_{x \in \Omega} \left(1 - \xi_{I_C}\right) \left[I_{\text{CTF},j} - I_{\text{CT},j} \left(x + \sum_{p=1}^{n} \text{DVF}_p(x) \cdot \mu_p^* + g(x) \right) \right]^2 + \xi_{I_C} \sum_{x \in \Omega} g\left(x^{\text{SI}}\right)^2, \tag{9}$$

where ξ_{I_C} is a set of adaptive variable coefficients, with $\xi_k = \left(R_{\text{CT},k} - R_{\text{CTF},k}\right) / R_{\text{CT},k}$ for the kth control node, where $R_{\text{CT},k}$ and $R_{\text{CTF},k}$ are the regions influenced by the kth node in the whole chest CT image and in the CTF image, respectively. If the region of influence of the kth control node lies outside the partial EE image, $\xi_k = 1$. Thus, the motion of this control node can be determined only from the prior information, and the final displacement in the SI direction is zero. Alternatively, if the influenced region exists entirely within the CTF image, $\xi_k = 0$, and the registration result is determined only by the intensity difference of the overlap between the two images in this region. Because the CTF and CT scan images are given, ξ_{I_C} will be determined before the registration process. Note that the value of $g(x)$ is related to the displacement of the control nodes and can be extracted from the deformation field, which is generated based on the B-spline registration algorithm and can be optimized by using the gradient descent method.

Results

Evaluation of the weighted sparse algorithm-based lung respiratory motion model

In the following study, the sectional CT scan from the EE phase was used to simulate the CTF image. For the weighted sparse model, the weighting parameters λ_1 and λ_2 in Eq. 5 are determined on 26 training subjects using the leave-one-out strategy. First, the initial value of λ_2 is held at 0 while the parameter λ_1 is optimized based on the gradient descent method. The value of λ_1 is then held back to seek the suitable parameter λ_2 which was employed to produce an appropriate value of λ_1 in the next iterative optimization process. Therefore, the best values of the parameters λ_1 and λ_2 are iteratively tuned. The optimization process was repeated until the variation in the average TRE value of all training subsets is less than 0.05 mm or the maximum number of iterations was met (set to 30). To demonstrate the sensitivity of the parameters, the variation of the average target registration error (TRE) with these parameters is shown in Fig. 4. The result shows that the model formulation method is weakly sensitive when

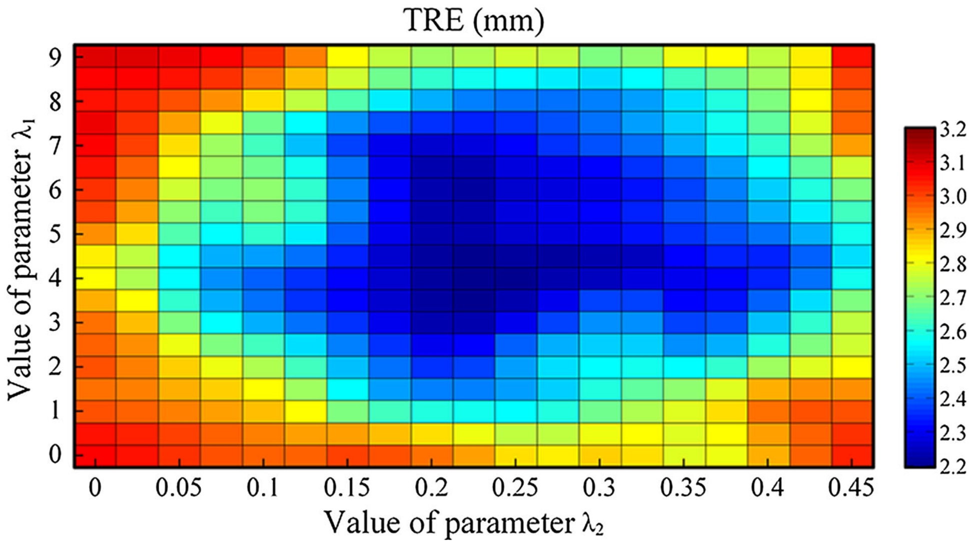

Fig. 4 The effect of the parameters on the average TRE for the training subsets

Table 1 Sample characteristics of datasets for each case

Data set	Breath type	Tidal volume (ml)	Average motion of landmark (mm)
01	Diaphragmatic	102.7	8.2
02	Diaphragmatic	131.4	9.6
03	Diaphragmatic	207.5	14.7
04	Thoracic	139.5	10.5
05	Thoracic	117.6	9.1
06	Thoracic	199.3	14.8
07	Thoracic	195.3	13.7
08	Thoracic	172.5	11.8
09	Mixed	194.6	14.3
10	Mixed	90.9	7.3

λ_1 is approximately 2–7 and λ_2 is between 0.1 and 0.4. We use $\lambda_1 = 4.5$ and $\lambda_2 = 0.2$ throughout our work because these values achieved the best TRE.

In this study, we collected data from 10 additional test subjects not included in the repository to evaluate the weighted sparse modelling method, as shown in Table 1. We compared the whole lung motion fields extracted using three state-of-the-art statistical lung motion model methods and the weighted sparse modelling method. The three methods considered for comparison are summarized as follows:

Method I MMM [7]. An average motion field was computed based on the motion fields extracted from the 26 training subjects (the details of these subjects can be found in "Data preparation" section) and was employed to deform the floating EI CT image. A scaling factor was used to control the amplitude of the average motion field. The optimal value of this scaling factor was optimally determined by minimizing the intensity difference between the deformed CT image and the reference CTF image in the CTF image space.

Method II PCA model [10]. The resulting DVFs for 26 training subjects form a matrix, where each column represents the whole DVF field for a corresponding subject. The traditional PCA was then performed on this matrix to calculate the eigenvectors and eigenvalues. A new displacement field was reconstructed by varying the PCA coefficient, with the objective of solving a deformation field to align the new input $I_{\mathrm{CT},j}$ to $I_{\mathrm{CTF},j}$. The PCA coefficients were optimized based on the image similarity in the region of overlap between the deformed $I_{\mathrm{CT},j}$ and $I_{\mathrm{CTF},j}$. We tested the effect of different numbers of principal components. The mean TRE values of the PCA method constructed by the first one (retained 85.2% variance), first two (retained 92.5% variance), first three (retained 95.4% variance), first four (retained 97.1% variance) and all PCA components were 2.9 mm, 3.0 mm, 2.7 mm, 2.8 mm and 3.4 mm, respectively. Furthermore, an improved PCA model, which achieved the best prediction accuracy (mean TRE = 2.6 mm), was formulated by penalizing the weights of all principal components and using the same $L1$ norm relaxation in Eq. 1.

Method III Exemplar population model [11]. For the training data used here, 4D CT datasets were acquired from 10 volunteers under free breathing. Ten phases were observed for each subject. For each test subject, approximately 100 landmarks were determined on the EI CT image using a semi-automatic tool [20], and the bifurcation points of the vessel were manually chosen. A registration method was applied to warp the EI CT image from each test subject onto the training CT images from each breathing phase. Then, the resultant deformation field was used to map the landmarks to their corresponding points in the training images to build the subject-specific PCA model. The population PCA model was constructed on all 4D CT data of all training subjects. Three of the landmarks for each test subject were used as the surrogates to calculate a series of weights based on the simi-

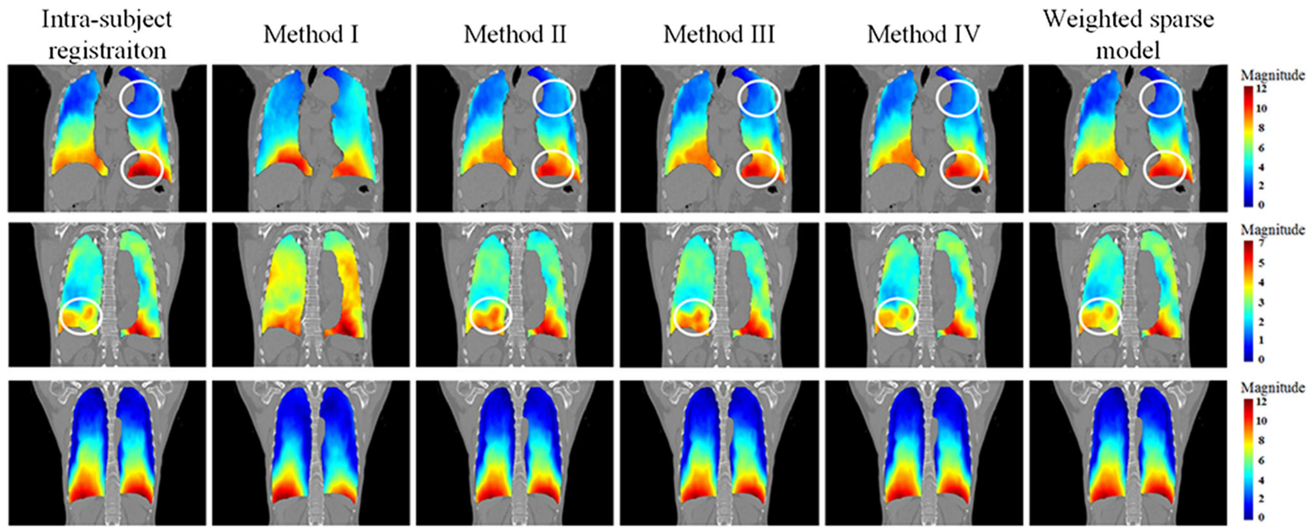

Fig. 5 Visualization of the computed intrasubject DVFs for three random subjects (one subject per row) between the EE and EI phases. The magnitude of the respiratory motion field is visualized and colour coded in millimetres (mm)

Table 2 TRE in mm of each method using manual expert landmarks

Dataset	Intrasubject registration	Method I	Method II	Method III	Method IV	Weighted sparse model (without *e* term)	Weighted sparse model (with *e* term)
01	1.2 (0.6)	4.8 (2.0)	2.4(1.1)	2.4 (1.0)	2.1 (1.0)	2.2 (1.1)	2.1 (0.9)
02	1.6 (0.8)	4.4 (2.1)	2.8 (1.0)	2.6 (1.2)	2.3 (1.0)	2.3 (1.0)	2.2 (1.0)
03	1.8 (1.2)	4.8 (2.5)	3.0 (1.6)	2.8 (1.5)	2.6 (1.4)	2.7 (1.4)	2.5 (1.3)
04	1.7 (0.9)	5.4 (2.6)	2.9 (1.3)	2.8 (1.3)	2.7 (1.1)	2.6 (1.2)	2.5 (1.0)
05	1.3 (0.6)	4.4 (2.4)	2.5 (1.1)	2.5 (1.1)	2.2 (1.0)	2.2 (1.0)	2.0 (1.0)
06	1.9 (1.3)	4.5 (2.9)	3.0 (1.6)	2.9 (1.6)	2.4 (1.5)	2.6 (1.5)	2.4 (1.4)
07	1.8 (1.0)	6.2 (3.9)	2.9 (1.4)	2.8 (1.5)	2.6 (1.4)	2.7 (1.6)	2.5 (1.4)
08	1.6 (0.8)	5.9 (3.6)	2.9 (1.4)	2.7 (1.2)	2.6 (1.1)	2.4 (1.2)	2.4 (1.0)
09	1.1 (0.6)	6.4 (3.6)	2.3 (1.2)	2.1 (1.1)	2.1 (1.0)	2.0 (1.0)	1.9 (0.9)
10	1.3 (0.9)	3.7 (2.0)	2.6 (1.3)	2.4 (1.1)	2.0 (1.0)	2.1 (1.2)	2.0 (0.9)
Mean	1.5 (0.9)	5.0 (2.4)	2.6 (1.4)	2.6 (1.3)	2.4 (1.2)	2.4 (1.2)	2.2 (1.1)

larity of the surrogate and the corresponding model. Finally, a weighted combination of all examples was formulated to predict the motion field.

Method IV Traditional sparse model. This model is constructed based on Eq. 1, and the resulting values of the sparse weights were optimized based on function (6).

Figure 5 presents a visual comparison of the results for first three test subjects. Notably, the result of the intrasubject registration [17] was calculated based on reference EE CT images and floating EI CT images and was employed as the ground truth for visual illustration of the motion prediction of the statistical motion model. Because the motion repository contained information on multiple types of respiration and only nine diaphragmatic respiration samples, Method I failed to accurately predict the motion information, as visualized in the second column of Fig. 5. In most lung regions, Method II, Method III and the proposed weighted sparse model recovered accurate deformation information. However, there was some local deformation information loss (white curves), as shown in the third and fourth columns of Fig. 5. For the three selected subjects, the weighted sparse modelling method achieved more accurate DVF information than the PCA method. Approximately 100 landmark pairs in the EE and EI CT images covering the whole lung region were manually obtained to evaluate the respiratory motion estimates. In Table 2, we list the average and standard deviation of the TRE [21] of these landmarks for the 10 test subjects and compare the motion prediction result achieved by the weight sparse model with and without the *e* term in Eq. 5. Note that the proposed weighted sparse motion model has less error compared with the other model methods. Compared with the traditional sparse model (Method IV), the proposed weighted sparse model employs a normalized diagonal matrix to prejudge the similarity between the

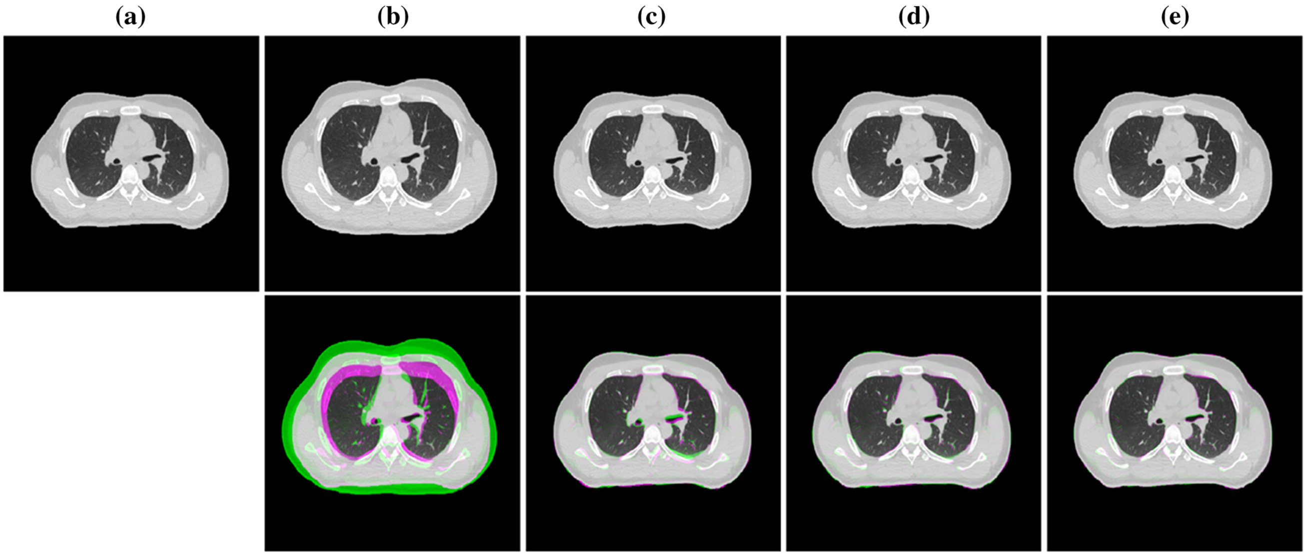

Fig. 6 Results of CT image registration: **a** CTF, **b** inhale CT, **c** weighted sparse model-based registration, **d** fast CT–CTF registration and **e** motion prior-based registration. The bottom row shows an overlay of the CTF (magenta) and deformed CT (green) images

Table 3 Comparison of the ASSD (mm) and TRE (mm) results for the vessel tree surface

Dataset	Weighted sparse model		Fast CT–CTF registration		Motion prior-based registration	
	TRE	ASSD	TRE	ASSD	TRE	ASSD
01	2.2 (1.2)	3.1 (1.5)	1.8 (0.9)	2.1 (1.1)	1.5 (0.4)	1.0 (0.5)
02	2.3 (1.3)	3.3 (1.4)	2.0 (0.9)	2.2 (1.2)	1.5 (0.7)	1.0 (0.7)
03	2.4 (1.2)	4.4 (1.9)	2.5 (1.3)	2.9 (1.9)	1.7 (1.0)	1.8 (0.8)
04	2.6 (1.2)	3.3 (1.5)	2.5 (1.2)	2.3 (1.1)	1.7 (0.8)	1.4 (0.6)
05	2.2 (1.4)	3.0 (1.5)	1.8 (0.9)	2.5 (1.2)	1.5 (0.7)	1.3 (0.6)
06	2.7 (1.6)	3.4 (1.7)	2.2 (1.2)	3.1 (1.2)	1.8 (0.8)	1.6 (0.6)
07	2.3 (1.5)	3.5 (1.9)	2.2 (1.3)	2.9 (1.4)	1.6 (1.0)	1.6 (0.5)
08	2.4 (1.1)	3.2 (1.7)	2.3 (1.0)	2.2 (1.3)	1.7 (0.6)	1.5 (0.7)
09	2.3 (1.3)	4.1 (2.2)	1.6 (1.0)	2.3 (1.7)	1.0 (0.7)	1.6 (0.6)
10	2.0 (1.0)	2.5 (1.5)	1.7 (0.9)	1.8 (0.8)	1.4 (0.8)	1.0 (0.6)
Mean	2.4 (1.3)	3.4 (1.7)	2.1 (1.2)	2.5 (1.2)	1.5 (0.8)	1.4 (0.6)

motion information of the new input patient and that of the training DVFs. Therefore, the weighted sparse model can more easily eliminate the influence of a dissimilar training DVF and achieve a better result (mean TRE = 2.2 mm) than the traditional model (mean TRE = 2.4 mm). The paired *t* test results showed that the proposed weighted sparse model with the *e* term is better than the four comparison methods and the proposed method without the *e* term in terms of the TRE metric (p value <0.05), respectively.

Evaluation of motion prior-based registration with adaptive variable coefficients

In this section, 15–20 landmark pairs in the CTF region were manually determined for each testing subject to evaluate the registration results between EI CT and simulated EE CTF images. We compared the performance of the weighted sparse model, fast CT–CTF registration with motion compensation [3], to that of the motion prior-based registration method throughout the CTF image volume, as shown in Fig. 6. For this comparison, the intermediate CT images proposed in [3] were generated by warping the floating EI CT images using the deformation field generated with the weighted sparse model. The average symmetric surface distance (ASSD) [22] of the vessel model and the TRE of the landmark pairs were used to quantitatively evaluate the final respiratory motion estimation results in the lung region contained by the CTF image (see Table 3). The proposed registration approach showing greater accuracy than the com-

Table 4 Mean landmark motion (mm) and mean TRE (mm) of the proposed motion prediction framework

Phase	1	2	3	4	5	6	7	8	9
Mean landmark motion	1.2 (1.1)	2.2 (2.3)	3.1 (3.3)	4.2 (4.1)	5.3 (4.8)	7.6 (6.9)	8.3 (7.5)	9.6 (8.1)	11.1 (9.5)
Mean TRE	0.2 (0.1)	0.4 (0.2)	0.5 (0.3)	0.7 (0.3)	0.8 (0.5)	1.1 (0.6)	1.2 (0.6)	1.3 (0.7)	1.6 (0.7)

parison approach (mean TRE = 1.6 mm, mean ASSD = 1.4 mm and p value <0.05).

Evaluation of the proposed motion model for 4D CT datasets

In clinical applications, motion estimates throughout the respiratory cycle are required. In this section, 4D CT image data from 10 subjects were employed to validate the proposed method at different time points throughout the breathing cycle. Each 4D CT dataset consisted of ten breathing phases. The CT scan from the EI phase was used as the floating CT image, and the sectional CT scan from the EE phase was used to simulate the CTF image (reference image). Thus, the proposed method can predict the respiratory motion based on the EI CT and EE CTF image pairs. The remaining breathing phases were employed to evaluate the accuracy of the motion model.

The locations of one landmark point in each intermediate CT images were employed to simulate the motion of the reference needle and used to drive the motion model. Since the location of this landmark is known in each intermediate CT image, the motion model can compute a similar location of this landmark, and the breathing time point can be determined. Then, the predicted locations of the remaining landmarks at this breath state were compared with their real locations in corresponding CT images. As listed in Table 4, the maximum TRE value was 1.6 (0.7) mm (with $\approx$ 20 landmark pairs) and occurred between the maximum inhale and the maximum exhale. The TRE usually increased by $\leq$ 1.4 mm with increasing magnitude of the landmark motion.

Discussion and Conclusions

In this study, we present a novel motion modelling technique based on a whole chest CT scan and a CTF scan of the ROI to construct a patient-specific local lung respiratory motion model for model-driven biopsies. The weighted sparse motion model, which is used to obtain the motion prior for the registration process, performs well in preserving detailed local motion information. We also introduce a motion prior-based registration method with adaptive weighting coefficients to address the error of the statistical motion model in the ROI by considering the relative influence of prior knowledge and image intensity information during the registration process.

Compared to previous work [10, 11], the weighted sparse model can provide more accurate motion prediction results. According to our experimental comparison, when the relevant local motion information is contained in only a minority of the training subjects in the motion repository, the respiratory motion estimates obtained using Method I are unsatisfactory. The PCA model constructed with the first several components can effectively reduce the inaccuracy in the deformation field of the training subjects, resulting in superior results (mean TRE <3.0 mm) compared with the model with all PCA components (mean TRE = 3.4 mm) [23]. In addition, the results showed that the resulting prediction accuracy was improved by approximately 0.1 mm compared with that of the PCA model with the first three components when we added the same $L1$ norm term to the traditional PCA method. The main reason is that this method can adaptively determine the optimal number of principal components for each specific testing subject. However, PCA derives a set of orthonormal bases (principle components) of the subspace by maximizing their variability, where the components are ranked in descending order of the variation in the training dataset. Imposing sparse constraints on all principal components tends to identify a compact subset to adequately reconstruct the original sample. The first several principal components would be included in the selected subset despite the sparse constraint. This approach degenerates to the classical PCA and achieves a performance inferior to that of the proposed method due to the loss of local motion details in the discarded PCA components.

In [24, 25], the optimal PCA weights were computed by optimizing an objective function of the image registration, such as the NMI similarity metric employed in [24]. A similar strategy adopted in Eq. 6 is employed to achieve the optimal sparse weights to formulate the statistical motion model in the proposed work. Furthermore, the proposed motion prior-based registration is used to improve the prediction accuracy of the ROI throughout the CTF image region. Although the CT–CTF registration task has been accomplished in a previous work [3], the proposed motion prior-based registration method has two advantages. First, the proposed method can be applied to a single CT image and an CTF image to complete the motion modelling task instead of requiring two CT scans and one CTF scan. Second, the regularization term $\sum_{x_i \in \Omega} g(x^{\mathrm{SI}})^2$ in function (9) is flexible by virtue of the proposed adaptive variable coefficients. The deformation of a control point is varied depending on whether the affected region is within the CTF region.

During the treatment, the motion model should deal with the motion variability, such as intra- and inter-breathing cycle variability. In "Evaluation of the proposed motion model for 4D CT datasets" section, 4D CT images were employed to evaluate the performance of the proposed motion prediction method for hysteresis in lung motion introduced by intra-cycle variability. The motion model was generated based on EI CT and EE CTF images and was driven by one of the landmark points to present the motion of the ROI at different time points throughout the inter-breathing cycle. The result indicated that the accuracy is sufficient for clinical percutaneous lung intervention, since it has been reported that an average TRE of less than 3.3 mm is sufficient for accomplishing the intervention task [3]. In addition, we proposed a clinical operation framework based on a lung motion model, an electromagnetic navigator and a pair of needles for percutaneous biopsy in our previous study [4]. Following this framework, the hysteresis phenomenon in the target region can be simulated based on the motion of a prepositioned reference needle as tracked by the electromagnetic navigator. Although the above framework can also alleviate the influence of inter-cycle variability, the motion model constructed from only two breath phases is not enough. To solve this problem, we aim to search for large amounts of 4D CT images in the future to formulate the motion model and analyse how the motion representation is related to surrogate signals, such as the motion of diaphragm positions and the body surface.

Although we employed an e term to solve the effect of the error introduced by the transformations $\varphi_{j\to 1}$ and $\varphi_{1\to p}$ in Eq. 1, this error may still be a main factor influencing the motion prediction performance. Instead of randomly choosing an image from the training dataset, a common intensity atlas may be a feasible way to address registration error. However, we need to solve the inverse transformation problem [7] after employing this atlas, which is an issue of focus in image registration algorithms because this task is usually subjected to inverse consistency error [26]. In future work, we plan to develop a suitable image atlas generation method and an efficient inverse consistency registration method to enhance the robustness of the proposed method with respect to noise.

Acknowledgements This research was partially supported by the National Natural Science Foundation of China (61902109), the Natural Science Foundation of Hebei Province (F2019205070 and F2017205066) and the Science Foundation of Hebei Normal University (L2019B01, L2017B06, L2019K01 and L2018K02).

Compliance with ethical standards

Conflict of interest The authors declare that they have no conflict of interest.

Ethical approval All procedures performed in studies involving human participants were in accordance with the 8 ethical standards of the institutional and/or national research committee and with the 1964 Helsinki Declaration and its later amendments or comparable ethical standards.

Informed consent Informed consent was obtained from all individual participants included in the study.

References

1. Dinh CV, Steenbergen P, Ghobadi G, van der Poel H, Heijmink SWTPJ, de Jong J, Isebaert S, Haustermans K, Lerut E, Oyen R, Ou Y, Christos D, van der Heide UA (2017) Multicenter validation of prostate tumor localization using multiparametric MRI and prior knowledge. Med Phys 44(3):949–961. https://doi.org/10.1002/mp.12086
2. Kuntz A, Torres LG, Feins RH, Webster RJ, Alterovitz R (2015) Motion planning for a three-stage multilumen transoral lung access system. In: IEEE International conference on intelligent robots and systems, pp 3255–3261. https://doi.org/10.1109/IROS.2015.7353829
3. Su P, Yang J, Lu K, Yu N, Wong ST, Xue Z (2013) A fast CT and CT-fluoroscopy registration algorithm with respiratory motion compensation for image-guided lung intervention. IEEE Trans Biomed Eng 60(7):2034–2041. https://doi.org/10.1109/TBME.2013.2245895
4. Chen D, Chen W, Huang L, Feng X, Peters T, Gu L (2017) BEM-based simulation of lung respiratory deformation for CT-guided biopsy. Int J Comput Assist Radiol Surg 12(9):1585–1597. https://doi.org/10.1007/s11548-017-1603-8
5. de Vos BD, Berendsen FF, Viergever MA, Staring M (2017) End-to-end unsupervised deformable image registration with a convolutional neural network. In: Lecture notes in computer science, vol 10553, pp 204–212. https://doi.org/10.1007/978-3-319-67558-9
6. Krebs J, Mansi T, Mailhé B, Ayache N, Delingette H (2018) Unsupervised probabilistic deformation modeling for robust diffeomorphic registration. In: Lecture notes in computer science, vol 11045, pp 101–109. https://doi.org/10.1007/978-3-030-00889-5_12
7. Ehrhardt J, Werner R, Schmidt-Richberg A, Handels H (2011) Statistical modeling of 4D respiratory lung motion using diffeomorphic image registration. IEEE Trans Med Imaging 30(2):251–265. https://doi.org/10.1109/TMI.2010.2076299
8. Blackall JM, Ahmad S, Miquel ME, McClelland JR, Landau DB, Hawkes DJ (2006) MRI-based measurements of respiratory motion variability and assessment of imaging strategies for radiotherapy planning. Phys Med Biol 51(17):4147–4169. https://doi.org/10.1088/0031-9155/51/17/003
9. Baumgartner CF, Kolbitsch C, McClelland JR, Rueckert D, King AP (2017) Autoadaptive motion modelling for MR-based respiratory motion estimation. Med Image Anal 35:83–100. https://doi.org/10.1016/j.media.2016.06.005
10. Ha IY, Wilms M, Handels H, Heinrich MP (2019) Model-based sparse-to-dense image registration for realtime respiratory motion estimation in image-guided interventions. IEEE Trans Biomed Eng 66(2):302–310. https://doi.org/10.1109/TBME.2018.2837387

11. Samei G, Tanner C, Székely G (2012) Predicting liver motion using exemplar models. In: Lecture notes in computer science, vol 7601, pp 147–157. https://doi.org/10.1007/978-3-642-33612-6_16
12. Li R, Lewis JH, Jia X, Zhao T, Liu W, Wuenschel S, Lamb J, Yang D, Low DA, Jiang SB (2011) On a PCA-based lung motion model. Phys Med Biol 56(18):6009–6030. https://doi.org/10.1088/0031-9155/56/18/015
13. Zhang S, Zhan Y, Dewan M, Huang J, Metaxas DN, Zhou XS (2012) Towards robust and effective shape modeling: sparse shape composition. Med Image Anal 16(1):265–277. https://doi.org/10.1016/j.media.2011.08.004
14. Yu Y, Zhang S, Li K, Metaxas D, Axel L (2014) Deformable models with sparsity constraints for cardiac motion analysis. Med Image Anal 18(6):927–937. https://doi.org/10.1016/j.media.2014.03.002
15. Wang T, Xie H, Zhang S, Chen D, Gu L (2018) A pulmonary deformation registration framework for biplane X-ray and CT using sparse motion composition. In: Proceedings of IEEE life sciences conference, pp 47–50. doi: 10.1109/LSC.2017.8268140 -
16. Chen D, Xie H, Zhang S, Gu L (2017) Lung respiration motion modeling: a sparse motion field presentation method using biplane X-ray images. Phys Med Biol 62(19):7855–7873. https://doi.org/10.1088/1361-6560/aa8841
17. Heinrich MP, Papiez BW, Schnabel JA, Handels H (2014) Non-parametric discrete registration with convex optimisation. In: Lecture notes in computer science, vol 8545, pp 51–61. https://doi.org/10.1007/978-3-319-08554-8_6
18. Cheng Y, Hu X, Wang J, Wang Y, Tamura S (2015) Accurate vessel segmentation with constrained B-snake. IEEE Trans Image Process 24(8):2440–2455. https://doi.org/10.1109/TIP.2015.2417683
19. Javaherian A, Holman S (2017) A multi-grid iterative method for photoacoustic tomography. IEEE Trans Med Imaging 36(3):696–706. https://doi.org/10.1109/TMI.2016.2625272
20. Murphy K, van Ginneken B, Klein S, Staring M, de Hoop BJ, Viergever MA, Pluim JPW (2011) Semi-automatic construction of reference standards for evaluation of image registration. Med Image Anal 15(1):71–84. https://doi.org/10.1016/j.media.2010.07.005
21. Qiu L, Zhang Y, Xu L, Niu X, Zhang Q, Zhang L (2018) Estimating maximum target registration error under uniform restriction of fiducial localization error in image guided system. IEEE Trans Med Imaging 37(4):881–892. https://doi.org/10.1109/TMI.2017.2776404
22. Feng Y, Dong F, Xia X, Hu CH, Fan Q, Hu Y, Gao M, Mutic S (2017) An adaptive fuzzy C-means method utilizing neighboring information for breast tumor segmentation in ultrasound images. Med Phys 44(7):3752–3760. https://doi.org/10.1002/mp.12350
23. Xu Y, Yan H, Ouyang L, Wang J, Zhou L, Cervino L, Jiang SB, Jia X (2015) A method for volumetric imaging in radiotherapy using single X-ray projection. Med Phys 42(5):2498–2509. https://doi.org/10.1118/1.4918577
24. Onofrey JA, Papademetris X, Staib LH (2015) Low-dimensional non-rigid image registration using statistical deformation models from semi-supervised training data. IEEE Trans Med Imaging 34(7):1522–1532. https://doi.org/10.1109/TMI.2015.2404572
25. Denis De Senneville B, El Hamidi A, Moonen C (2015) A direct PCA-based approach for real-time description of physiological organ deformations. IEEE Trans Med Imaging 34(3):974–982. https://doi.org/10.1109/TMI.2014.2371995
26. Zhang Y, Tehrani JN, Wang J (2017) A biomechanical modeling guided CBCT estimation technique. IEEE Trans Med Imaging 36(2):641–652. https://doi.org/10.1109/TMI.2016.2623745

Publisher's Note Springer Nature remains neutral with regard to jurisdictional claims in published maps and institutional affiliations.